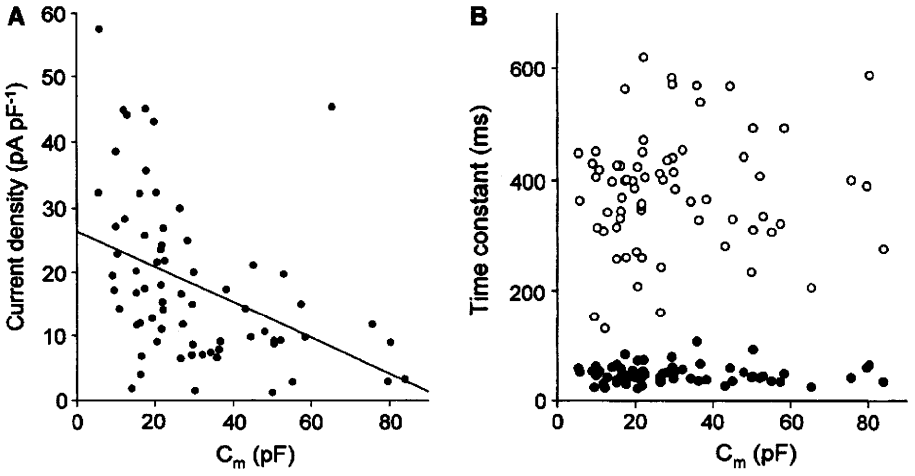

Fig. 4 Relationships between HL-1 cell size and E-4031-sensitive current. Scatter plots of the current density (**a**) and the deactivation time constants (**b**) of the slow (*open circles*) and fast (*filled circles*) components, measured in E-4031-sensitive tail current elicited by a voltage step to −50 mV after 1-s depolarization to +20 mV, against the membrane capacitance of individual cells. Data were obtained from HL-1 cells (passages 38–52)

1.2 and 57.5 pA pF^{-1} (18.1 ± 1.5 pA pF^{-1}, $n = 69$), which was roughly and negatively correlated with cell size ($r = -0.42$, $P < 0.0003$). On the other hand, no obvious correlation between deactivation kinetics of I_{Kr} and cell size was observed (Fig. 4b).

Voltage Dependence of I_{Kr} Inactivation in HL-1 Cells

The shape of the I_{Kr} tail current (initial "hook" or increase in amplitude, followed by slower decay) reflects the presence of a biphasic process during repolarization. The initial increasing phase of the tail current preceding a decay in amplitude has been shown to reflect a recovery from inactivation that occurs much faster than deactivation (Sanguinetti and Jurkiewicz 1990; Shibasaki 1987). In Fig. 5, the rate of recovery from inactivation was estimated. The currents were elicited by voltage pulses to various test potentials between −120 and −10 mV after the 1-s preconditioning pulses to +20 mV. Experiments were conducted at 25°C to allow discrimination of the onset of tail currents from capacitive transients. In Fig. 5a, a set of current traces during test steps is shown. Increment phases of the tail current were well fitted by a single-exponential function with smaller time constants at more negative potentials. For example, the averaged τ value at −120 mV was 0.92 ± 0.04 ms, while it increased to 10.50 ± 0.74 ms at −10 mV (Fig. 5b).

The voltage dependence of current inactivation was examined using a three-pulse protocol (inset in Fig. 6a) (Smith et al. 1996), in which the cell was depolarized to +20 mV for 1 s to activate and inactivate I_{Kr} channels,

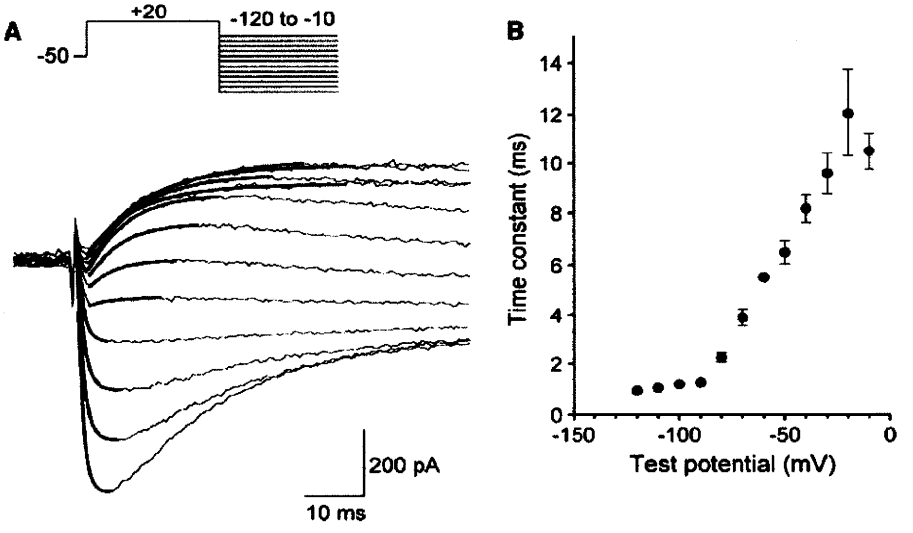

Fig. 5 Kinetic properties of recovery from inactivation. **a** The "hook" tail currents (*thin line*) elicited by voltage steps to various potentials between −120 and −10 mV in 10-mV intervals following the 1-s depolarizing steps to +20 mV (*inset*). Current recording was conducted at 25°C. *Smooth curves* (*thick line*), superimposed to initial increasing phase in amplitude, are obtained by a single-exponential fit. **b** Voltage dependence of the rate of recovery from inactivation. Time constants, measured in (**a**), were plotted against each test potential. Values represent mean ± SEM of four cells (passages 41, 42)

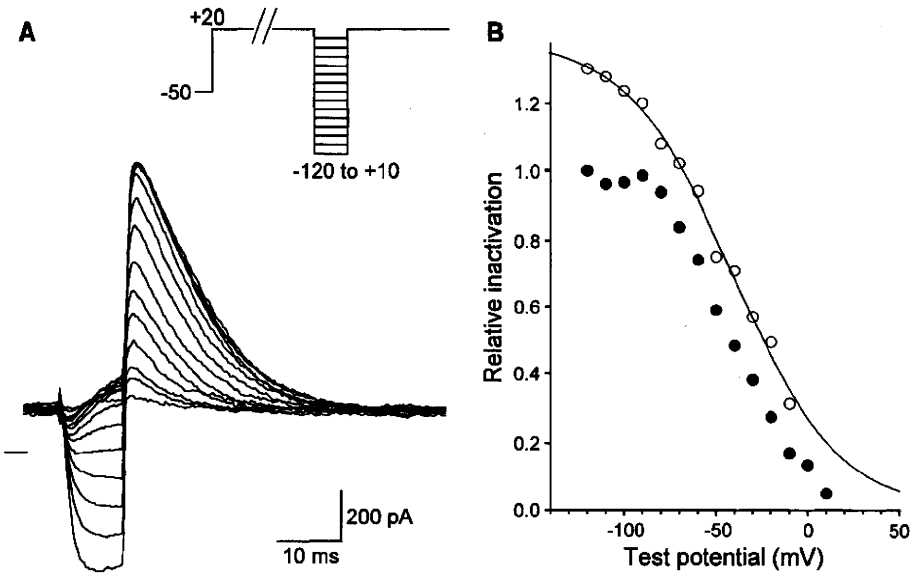

Fig. 6 Voltage dependence of steady-state inactivation. **a** E-4031-sensitive current recorded from an HL-1 cell (passage 41) in response to three-pulse protocol (*inset*). At first, a depolarizing pulse of more than 1 s duration to +20 mV (P1) was applied, where current was activated and inactivated rapidly. Then, a hyperpolarizing test pulse of 10 ms to a varied potential (P2) was used to allow recovery from inactivation, followed by a step to +20 mV (P3). *Dashed line* represents zero current level. Current recording was conducted at 25°C. **b** Current amplitude in response to the P3 pulse (*filled circles*) was normalized to the maximal amplitude at −120 mV and plotted against the test potentials. At negative voltages (≤−60 mV), significant deactivation occurred during 10 ms of the P2 repolarizing step. In addition, at less negative potential (>−70 mV), increasing phase current did not reach the steady-state level during the P2 step. Therefore, the fractional deactivation and incomplete recovery from inactivation during 10 ms were calculated using kinetic parameters (obtained from current traces in Fig. 5), and the data points were corrected to the steady-state inactivation level (*open circles*). Corrected values were well fitted by the Boltzmann equation (*smooth curve*)

then briefly (10 ms) repolarized to various test potentials between −120 and +10 mV to allow for recovery from inactivation without significant deactivation of the channels. After the brief steps, a depolarizing step to +20 mV was applied to evaluate the relative number of opening channels. Figure 6a shows a part of the current traces in response to the pulse protocol (as indicated in the inset). During the brief repolarization, the currents relaxed rapidly to the appropriate level to the corresponding test potentials. Then, depolarizing pulses to +20 mV elicited a large amplitude of outward currents that decayed to the steady-state level within 40 ms due to rapid inactivation. The peak amplitude of the outward currents was measured and plotted against test potentials as filled circles in Fig. 6b. Smith et al. (1996) described that the current amplitude at negative voltages (≤−60 mV) should be corrected because fast deactivation occurred during the brief repolarization. Furthermore, the recovery from inactivation also might not reach the steady-state level at depolarized potential (>−70 mV). Thus, the fractional deactivation and recovery from inactivation during 10-ms repolarizing steps were corrected with respect to the steady-state inactivation level (open circle in Fig. 6b). The half-maximal inactivation voltage calculated by fitting the corrected data to a Boltzmann function was −41.2 mV and the slope factor was 28.9 mV.

K^+ Permeability of I_{Kr} in HL-1 Cells

In Fig. 7, the effects of $[K^+]_o$ on the reversal potential (E_{rev}) of the tail current were investigated. Cells were bathed in Tyrode solution containing 2, 5.4 (normal) and 10 mM KCl; and tail currents were recorded at various test potentials between −120 and 0 mV in 10-mV steps following the 1-s preconditioning pulses to +20 mV (Fig. 7a). The tail current amplitudes were measured and plotted against test potentials in Fig. 7b. At all $[K^+]_o$ conditions, the current–voltage relationships were nearly linear at the potential range between −140 and −80 mV and prominent inward rectification was observed at more positive potential than −70 mV. The conductance at potentials between −140 and −80 mV, measured by fitting lines with a liner regression, was increased with incremental change in $[K^+]_o$ (10.6, 14.1 and 19.7 pS at 2, 5.4 and 10 mM $[K^+]_o$, respectively). E_{rev}, where the polarity of the tail current is reversed, was obtained from a linear regression of the data points between −140 and −70 mV. E_{rev} values at 2, 5.4 and 10 mM $[K^+]_o$ were −115, −91 and −76 mV, respectively, very near the calculated

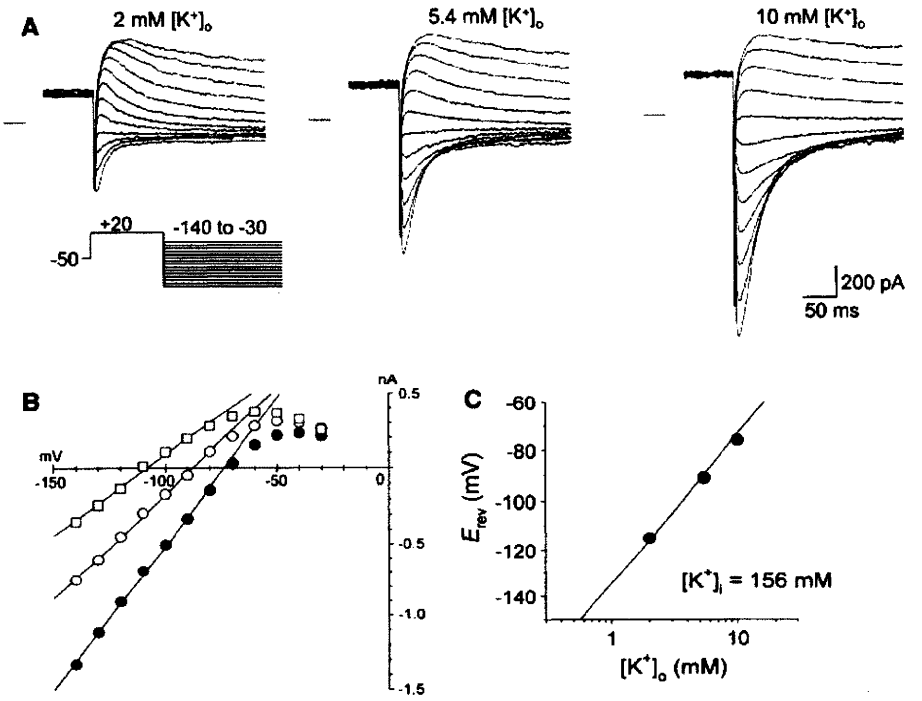

Fig. 7 Effects of extracellular K^+ concentrations on E-4031-sensitive currents. **a** Tail currents recorded at 2 (*left*), 5.4 (*middle*) and 10 mM $[K^+]_o$ conditions (*right*) at 25°C. The cell (passage 39) was initially depolarized to +20 mV from a holding potential of −50 mV, followed by test steps to various potentials between −120 and −30 mV (voltage protocol, *inset*). **b** Tail current amplitude at 2 (*open squares*), 5.4 (*open circles*) and 10 mM $[K^+]_o$ conditions (*filled circles*) shown as a function of test potentials. *Solid lines* on the plot were obtained by a linear regression of data points between −140 and −70 mV: $I_{tail} = g_{max} \cdot (E - E_{rev})$, where g_{max} and E_{rev} were, respectively, 10.6 pS and −115 mV at 2 mM $[K^+]_o$, 14.1 pS and −91 mV at 5.4 mM $[K^+]_o$ and 19.7 pS and −76 mV at 10 mM $[K^+]_o$. **c** Relationships between $[K^+]_o$ and E_{rev}. E_{rev} values in (**b**), plotted against each $[K^+]_o$ concentration, were in good agreement with a predicted E_K (*solid line*) calculated using a Nernst equation, $E_K = RT/F \cdot \ln([K^+]_o/[K^+]_i)$, where $[K^+]_i$ was assumed to be 158 mM

equilibrium potential of K^+ of −116, −89 and −73 mV, respectively (Fig. 7c).

Blocking Effects of E-4031 and Dofetilide on I_{Kr} in HL-1 Cells

In Fig. 8, the blocking effects of methanesulfonanilide drugs E-4031 and dofetilide on I_{Kr} in HL-1 cells were determined. The 1-s depolarizing pulses to +20 mV were repetitively given to the cells every 8 s to activate I_{Kr}, and the blocking effects of the drugs were determined by reduction of tail current elicited at −50 mV. Figure 8a shows the time course of changes in tail current amplitude during application of E-4031 at various concentrations as indicated. In the absence of drugs, the magnitude of the tail current was stable. Exposure to 10 nM E-4031 gradually reduced the tail currents by about 20% at the steady-state level, and the blocking effects increased as the drug concentration became higher. The IC_{50} values for block of tail currents by dofetilide and E-4031 were estimated to be 15.1 and 21.2 nM, respectively; and both drugs inhibited tail current completely at 1 μM (Fig. 8b, c).

Mouse ERG1 Expression Underlies I_{Kr} in HL-1 Cells

In Fig. 9, mERG1 expression in HL-1 cells was investigated with RT-PCR and Western blot assay. It has been reported that there are at least three isoforms of ERG1 at the mRNA level in human and mouse, i.e., the full-length ERG1a and two alternative splicing variants, ERG1a′ and ERG1b, with shorter N termini (Lees-Miller et al. 1997; London et al. 1997). In the present study, therefore, primer pairs directed to each ERG1 isoform were used for PCR amplification. Figure 9a shows an agarose gel of amplified PCR products, where specific bands of the expected size are detected for mERG1a (747 bp), mERG1a′ (755 bp) and mERG1b (1,109 bp) only in the presence of transcriptase. A similar gene expression profile was also detected in adult mouse atrial tissue (Fig. 9b). In order to examine protein expression, we employed an anti-ERG1 antibody that recognizes a common C-terminal epitope in all three mERG1 isoforms. As shown in Fig. 9c, the C-terminal ERG1 antibody identified several bands on a Western blot of HL-1 cells. The two higher bands with molecular mass of 120 and 160 kDa are consistent with maturely

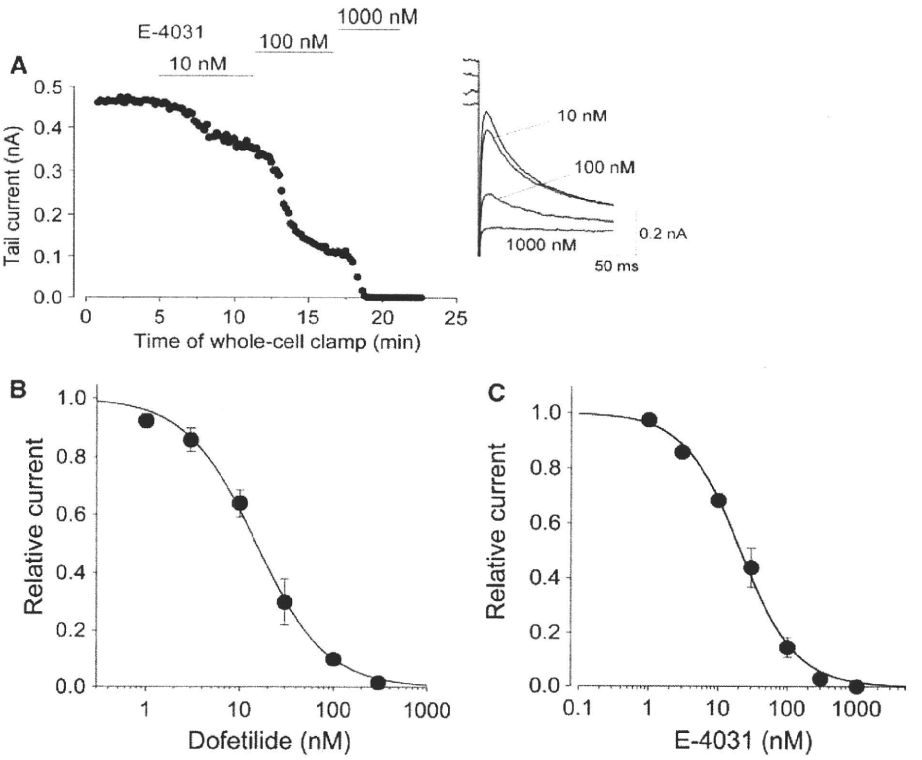

Fig. 8 Inhibitory effects of E-4031 and dofetilide on I_{Kr} in HL-1 cells. **a** Time course of changes in tail current amplitude during exposure to E-4031. Tail currents, as shown in *inset*, were elicited by a voltage step to −50 mV after 1-s depolarization to +20 mV. E-4031 was applied at various concentrations as indicated. **b**, **c** Dose-response relationships of blocking effects of E-4031 (**b**) and dofetilide (**c**). Tail current amplitude was normalized to the maximal amplitude in the absence of drug and plotted against each drug concentration. Data points represent mean ± SEM of five cells (passages 41–52). *Smooth curve* was obtained by fitting the data with a Hill equation, where IC_{50} and Hill coefficient were, respectively, 15.1 nM and 1.2 in (**b**) and 21.2 nM and 1.0 in (**c**)

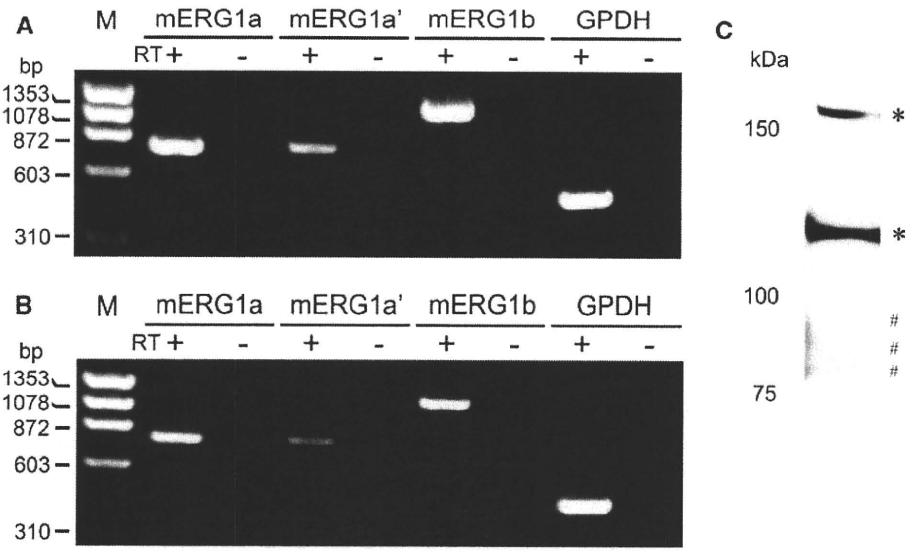

Fig. 9 Expression of mouse ERG1 isoforms in HL-1 cells and mouse atrium. PCR products amplified from cDNA derived from HL-1 cells culture (passage 40) (**a**) and atrial tissues dissected from adult mice (**b**), using primer pairs directed to mERG1a, mERG1a′ or mERG1b. *M* indicates a molecular maker of ϕX174/*Hae*III digest. **c** Western blot of total protein extracts from HL-1 cells (passages 45–47). Blotting with an antibody specific for ERG1 shows two mERG1a glycoform bands (*) at 120 and 160 kDa as well as three mERG1b glycoform bands (#) at 80, 87 and 93 kDa

glycosylated and unglycosylated ERG1a, respectively, in rat and canine ventricular myocytes (Jones et al. 2004), although contamination of signal attributed to ERG1a′ may be possible because of a small difference (~6 kDa) in protein size. On the other hand, we did observe three faint bands with lower molecular mass of 80, 87 and 93 kDa, which are consistent with bands attributed to different glycosylated forms of ERG1b in human and canine ventricular myocytes (Jones et al. 2004) and K562 human leukemic cells (Cavarra et al. 2007).

Recently, gene silencing by RNAi has become a broadly used technology for exploring gene function (Hannon 2002). In the present study, the functional relevance of mERG1 gene expression in HL-1 cells was determined using the RNAi technique. Two siRNA duplex oligonucleotides against all isoforms of mERG1 and ncRNA were

individually transfected into HL-1 cells together with a plasmid vector encoding GFP. Transfection efficacy estimated with green fluorescence was very low (≤5%), which never allowed us to detect an obvious decrease in mERG1 transcripts or proteins at the culture level (data not shown). However, the effects of siRNA were evident in whole-cell membrane current recorded from single GFP-positive cells. Compared to recordings in cells transfected with GFP alone (Fig. 10a), a much smaller time-dependent outward current was observed in cells transfected with siRNA, apparently due to a marked decrease in I_{Kr} amplitude (Fig. 10c, d). The effect of siRNA was attributable to specific knockdown of mERG1 expression because cells transfected with scRNA displayed currents with comparable amplitude to those recorded from cells transfected with GFP alone (Fig. 10b). I_{Kr} density determined by tail current elicited at −50 mV after the 1-s voltage steps to +30 mV was 1.95 ± 0.31 and 1.2 ± 0.34 pA pF^{-1} in cells transfected with siRNA-1 and siRNA-2, respectively. Both values were significantly smaller than those obtained from cells transfected with GFP alone (19.15 ± 2.34 pA pF^{-1}, $P < 0.01$) or with ncRNA (19.00 ± 2.69 pA pF^{-1}, $P < 0.01$) (Fig. 10e).

Discussion

In this article we describe the basic biophysical properties and molecular identity of I_{Kr} channels in HL-1 cells, the unique murine cardiac cell line established by Claycomb et al. (1998). Our current recordings demonstrated that most of the outward conductance in these cells was dominated by E-4031-sensitive current, which exhibited comparable characteristics to I_{Kr} in native mammalian cardiac cells, i.e., voltage- and time-dependent activation, prominent inward rectification, high K^+ permeability and nanomolar sensitivity to dofetilide or E-4031. In addition, we found that HL-1 cells possessed multiple transcripts and

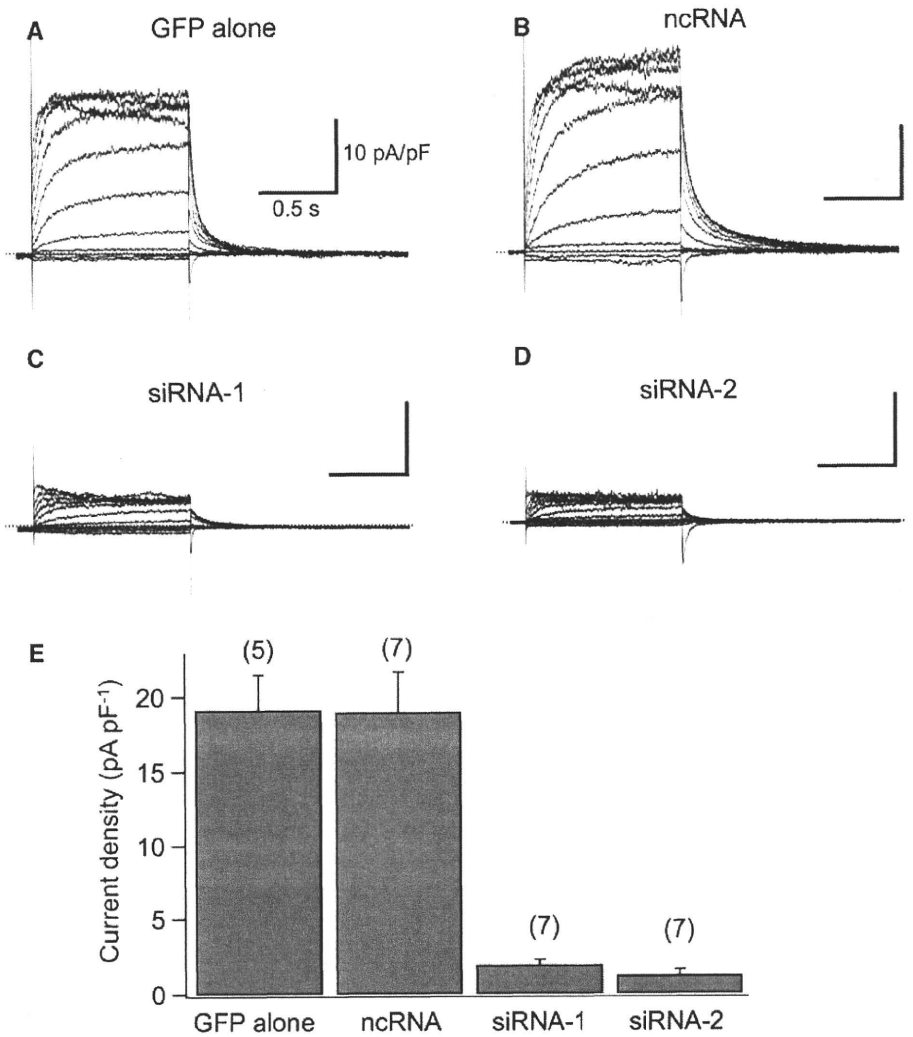

Fig. 10 Knockdown of mouse ERG1 with siRNA in HL-1 cells. Typical current traces recorded from HL-1 cells (passages 40, 41) transfected with GFP alone (**a**), GFP and nonspecific ncRNA (**b**), GFP and siRNA-1 (**c**) and GFP and siRNA-2 (**d**). Cell was held at −50 mV and given 1-s voltage steps to various potentials between −80 mV and +40 mV. **e** Bar graph displaying I_{Kr} density in each group (GFP alone, $n = 5$; GFP plus ncRNA, $n = 7$; GFP plus siRNA-1, $n = 7$; GFP plus siRNA-2, $n = 7$). Tail current was elicited upon repolarization to −50 mV following the 1-s depolarizing steps to +30 mV

proteins for the mouse ERG1 gene, known as molecular candidates underlying I_{Kr}. These findings indicate that HL-1 cells are a preferable source of native I_{Kr} channels.

Biophysical and Pharmacological Properties of I_{Kr} in HL-1 Cells

The biophysical profile of I_{Kr} channels is responsible for their specific role in cardiac action potential. The inward rectification mediated by a rapid voltage-dependent inactivation of channels suppresses current during the depolarizing phase of cardiac action potential, while a rapid recovery from inactivation followed by slow deactivation evokes a resurgent current during phase III repolarization. These unique gating properties have been extensively investigated in HERG channels. However, despite its physiological importance, relatively little information on cardiac I_{Kr} channels is available due to technical difficulties; i.e., significant current magnitude and minimal contamination of other time-dependent K^+ currents are required for reliable measurements. Current recordings in HL-1 cells potentially satisfied these requirements, which allowed us to evaluate the electrophysiological properties of I_{Kr} channels comprehensively. One possible limitation in our I_{Kr} recordings was that a holding potential of −50 mV was used to avoid contamination of $I_{Ca,T}$ (Xia et al. 2004) and I_f (Sartiani et al. 2002), which might affect I_{Kr} kinetic parameters and drug sensitivity because a significant fraction of channels were restrained in the inactivated state at −50 mV (see Fig. 6). Nevertheless, our recordings are similar to ones applying common protocols for the recording of native I_{Kr} in cardiomyocytes; thus, it is possible to draw a comparison between our results and those of earlier studies.

Voltage dependence of I_{Kr} activation in HL-1 cells was determined by two parameters, $V_{1/2}$ of −20.4 mV and k of 8.0 mV, which are practically consistent with the values previously reported for cardiac I_{Kr} in various mammals (Clark et al. 2004; Matsuura et al. 2002; Ono and Ito 1995; Sanguinetti and Jurkiewicz 1990). The deactivation kinetics of I_{Kr} varies between species. It is fast in guinea pig (Sanguinetti and Jurkiewicz 1990), while it is extremely slow in dog and cat (Barajas-Martínez et al. 2000; Liu and Antzelevitch 1995). In the present study, deactivation time constants were 46 ms for τ_{fast} and 438 ms for τ_{slow} at −50 mV when fitted to a double-exponential function, which are very similar to recent observation in mouse SA node cells (τ_{fast} and τ_{slow} were 40–70 ms and 400–600 ms at −50 mV, respectively) (Clark et al. 2004). Recovery from inactivation was very rapid even at 25°C, and time constants obtained in HL-1 cells were comparable to previous data for I_{Kr} in ferret atrial cells (Liu et al. 1996) but considerably smaller than the observation for HERG currents (Sanguinetti et al. 1995). We also determined the voltage dependence of steady-state inactivation of I_{Kr} channels using a three-pulse protocol that has been employed for HERG currents (Smith et al. 1996). The $V_{0.5}$ of −41.2 mV obtained in our analysis was very far from the value with HERG current (−90 mV) (Smith et al. 1996) but relatively similar to the value estimated by other methods in guinea pig or ferret (Liu et al. 1996; Sanguinetti and Jurkiewicz 1990), suggesting fundamental differences between cardiac I_{Kr} and HERG current in inactivation properties. Taken together, HL-1 cells appear to retain species-specific features of native I_{Kr}.

The sensitivity of I_{Kr} in HL-1 cells to E-4031 (IC_{50} 21.1 nM) was similar to that reported for native I_{Kr} in ferret and guinea pig cardiomyocytes (IC_{50} ~10 nM) (Liu et al. 1996; Weerapura et al. 2002). Dofetilide sensitivity observed in the present study (IC_{50} 15.1 nM) was also comparable with the values reported for native I_{Kr} in rabbit and guinea pig cardiomyocytes (IC_{50} 4–9 nM) (Carmeliet 1992; Weerapura et al. 2002). The sensitivity of the HERG channel to these compounds varies among expression systems. The channel expressed in *Xenopus* oocytes displays much lower sensitivity (E-4031 IC_{50} ~1 μM) (Sanguinetti et al. 1995), possibly due to yolk sac absorption of drugs in oocytes (Weerapura et al. 2002). On the other hand, in mammalian cell lines such as HEK cells and CHO cells, the IC_{50} values for the inhibition of HERG channel by E-4031 and dofetilide were reported to be 7.7 and ~10 nM, respectively (Zhou et al. 1998; Weerapura et al. 2002), which are indistinguishable from those previously reported for native I_{Kr} as well as our observation in HL-1 cells. Since inhibition of I_{Kr} is the predominant adverse effect of a diverse range of therapeutic agents (resulting in life-threatening proarrhythmic activity), assay of I_{Kr} in HL-1 cells may serve as a convenient preclinical tool to detect potential arrhythmogenic properties of any compound intended to be used as human medicine.

HL-1 Cells Possess Electrophysiological Properties Resembling Embryonic Phenotypes

Cardiac I_K is known to comprise at least two components, I_{Kr} and I_{Ks}, in various mammals. In HL-1 cells, however, I_{Kr} seems to be the sole I_K component. Indeed, a time-dependent outward current was almost totally abolished by application of E-4031 (Fig. 1). In mouse ventricular myocytes, the expression level of I_{Kr} and I_{Ks} is dependent on the developmental stage (Wang and Duff 1996; Wang et al. 1996); i.e., I_{Kr} is the predominant component of I_K in embryonic and fetal mice but is decreased during early postnatal development, whereas I_{Ks} is increased and both currents almost disappear in adult mouse. Along with these finding, the I_{Kr} expression pattern of HL-1 cells appears to

be similar to that of immature fetal mouse myocytes rather than well-differentiated adult mouse myocytes, although they derived from adult mouse hearts. Similarly, a fetal-type electrophysiological phenotype of HL-1 cells has been indicated by the expression of I_f and $I_{Ca,T}$ (Sartiani et al. 2002; Xia et al. 2004), which are known to be manifested in ventricular myocytes only at early embryonic stages (Niwa et al. 2004; Yasui et al. 2001).

HL-1 cells are known to beat when grown at proper density, again resembling embryonic cardiomyocytes. The spontaneous contractile activity, however, occurs in a restricted region of culture (Sartiani et al. 2002), suggesting heterogeneity of the functional expression level of ion channels in HL-1 cells. In fact, I_f was observed in only ~30% of HL-1 cells (Sartiani et al. 2002). Interestingly, the presence of both $I_{Ca,L}$ and $I_{Ca,T}$ had similar incidence (Xia et al. 2004). The limited expression of these membrane currents seems to be in agreement with the partial (local) occurrence of spontaneous beating in HL-1 cell culture because they play crucial roles in cardiac pacemaker activity. In the present study, I_{Kr} was recorded in almost all cells tested, even in quiescent HL-1 cells, while the current density of I_{Kr} was roughly and significantly correlated with cell size (Fig. 4). It has been suggested that a cell size-dependent difference in expression level of various ionic currents underlies the regional difference in electrical activity of rabbit SA node (Honjo et al. 1996; Lei et al. 2001). Although the relationship between spontaneous activity and the size of HL-1 cells is not known, it may be that the expression level of I_{Kr} channels is involved in the capability of spontaneous beating in HL-1 cell culture.

Molecular Basis of I_{Kr} in HL-1 Cells

The molecular basis of native I_{Kr} channel is still in debate. Although there is little doubt that the ERG1 gene underlies I_{Kr} channels in the heart, the reconstituted HERG channel displays much slower deactivation kinetics than native I_{Kr} channels (Sanguinetti et al. 1995). For this reason, auxiliary subunits such as KCNE1 and KCNE2 have been implicated as functional regulators of HERG channel (Abbott et al. 1999; McDonald et al. 1997). According to our preliminary experiments, we detected mRNA for KCNE1 from HL-1 cells, consistent with previous observations in AT-1 cells (Yang et al. 1994), but failed to find obvious expression of KCNE2 (data not shown). On the other hand, N-terminal splice variants of the ERG1 gene have been cloned in mouse and human and suggested to generate functional diversity of native I_{Kr} channels (Lees-Miller et al. 1997; London et al. 1997). The importance of these variants in the human heart was recently highlighted by the finding of a HERG1b-specific missense mutation associated with long QT syndrome (Sale et al. 2008). The N-terminal region of ERG1 contains the Per-Arnt-Sim (PAS) domain, which plays a crucial role in the slow deactivation process of the channel (Morais Cabral et al. 1998). The ERG1b isoform, which lacks the PAS domain in its truncated N terminus, exhibits faster deactivation than the full-length ERG1a (London et al. 1997), although its surface expression is not efficient unless coassembled with ERG1a (Phartiyal et al. 2007). In heterologous systems, coexpression of ERG1a and ERG1b leads to formation of a functional heterotetrameric channel with deactivation properties that more closely resemble native I_{Kr} than the channels produced by the expression of these isoforms individually (London et al. 1997). In fact, the deactivation time course of I_{Kr} in HL-1 cells was more similar to that reported for the mERG1a/1b channels rather than the mERG1a homomeric channel (e.g., τ_{fast} and τ_{slow} at −50 mV were 46 and 438 ms, respectively, in our experiments compared to 400–500 and ~2,000 ms, respectively, in mERG1a channel and 70–80 and 400–600 ms, respectively, in mERG1a/1b channel [London et al. 1997]). In the present study, we also confirmed the expression of both mERG1a and mERG1b in HL-1 cells, supporting the possible contribution of these isoforms in producing I_{Kr} in HL-1 cells. However, despite the abundance of transcripts, the protein bands for mERG1b were much weaker than those for mERG1a in our immunoblot analysis using an antibody that recognizes the common C-terminal epitope in both isoforms (Fig. 9). This might be attributable to differential accessibility of antibody to the common epitope in mERG1a and mERG1b (Jones et al. 2004). In mammalian heart, ERG1b protein expression has been clearly demonstrated using an isoform-specific antibody (Jones et al. 2004), whereas the antibodies against a common epitope recognized only ERG1a protein but failed to detect ERG1b (Pond et al. 2000). Further experiments are required to clarify the relative contribution of the mERG1b isoform to the generation of I_{Kr} in HL-1 cells.

Recently, siRNA has proven to be a powerful tool for investigating gene function by inducing knockdown phenotypes (Hannon 2002). In the present study, siRNA-mediated knockdown of mERG1 resulted in a dramatic decrease in I_{Kr}, providing direct evidence for an essential role of the mERG1 gene in the generation of I_{Kr} in HL-1 cells. It is possible to design siRNA for each isoform of mERG1 by targeting a specific exon sequence. Thus, our siRNA experiments suggested its potential application to the identification of gene products responsible for forming I_{Kr} in HL-1 cells. A major limitation of this approach was the difficulty of siRNA delivery into HL-1 cells. Our transfection efficiency using cationic lipids was <5%, which was sufficient for patch-clamp study but inadequate for biochemical analysis including measurements of mRNA and protein levels.

HL-1 Cells Are a More Reliable Source of I_{Kr} than AT-1 Cells

The electrophysiological characteristics of HL-1 cells seem to be qualitatively similar to those previously reported in their progenitor, AT-1 cells (Yang et al. 1994), except that the I_{Kr} density obtained from HL-1 cells in the present study (18 pA pF^{-1}) is three to four times larger than the value reported for AT-1 cells ($\sim$5 pA pF^{-1}) (Yang et al. 1994). Most importantly, they are quite different in their growth in culture. AT-1 cells proliferate to some extent in vitro, while extremely increasing their cell size, which is accompanied by changes in I_{Kr} density during primary culture (Yang et al. 1995). On the contrary, HL-1 cells can divide indefinitely in culture, while retaining their phenotype during continuous passages (Claycomb et al. 1998). In conclusion, taking advantage of their proliferative ability and stability of phenotype in culture, HL-1 cells can be adapted not only for electrophysiological experiments but also for biochemical and molecular biological experiments that require long-term culturing and provide a useful cardiac model for studies on the gating mechanisms, regulation by various signaling pathways, drug block and molecular basis of native I_{Kr} channels.

Acknowledgements This study was supported by a Grant-in Aid for Scientific Research from the Japan Society for the Promotion of Science. We are grateful to Dr. W. C. Claycomb for providing HL-1 cells.

References

Abbott GW, Sesti F, Splawski I et al (1999) MiRP1 forms I_{Kr} potassium channels with HERG and is associated with cardiac arrhythmia. Cell 97:175–187

Barajas-Martínez H, Elizalde A, Sánchez-Chapula JA (2000) Developmental differences in delayed rectifying outward current in feline ventricular myocytes. Am J Physiol 278:H484–H492

Carmeliet E (1992) Voltage- and time-dependent block of the delayed K^+ current in cardiac myocytes by dofetilide. J Pharmacol Exp Ther 262:809–817

Cavarra MS, del Mónaco SM, Assef YA et al (2007) HERG currents in native K562 leukemic cells. J Membr Biol 219:49–61

Chomczynski P, Sacchi N (1987) Single-step method of RNA isolation by acid guanidinium thiocyanate-phenol-chloroform extraction. Anal Biochem 162:156–159

Clark RB, Mangoni ME, Lueger A et al (2004) A rapidly activating delayed rectifier K^+ current regulates pacemaker activity in adult mouse sinoatrial node cells. Am J Physiol 286:H1757–H1766

Claycomb WC, Lanson NA Jr, Stallworth BS et al (1998) HL-1 cells: a cardiac muscle cell line that contracts and retains phenotypic characteristics of the adult cardiomyocyte. Proc Natl Acad Sci USA 95:2979–2984

Curran ME, Splawski I, Timothy KW et al (1995) A molecular basis for cardiac arrhythmia: *HERG* mutations cause long QT syndrome. Cell 80:795–803

Delcarpio JB, Lanson NA Jr, Field LJ et al (1991) Morphological characterization of cardiomyocytes isolated from a transplantable cardiac tumor derived from transgenic mouse atria (AT-1 cells). Circ Res 69:1591–1600

Field LJ (1988) Atrial natriuretic factor-SV40 T antigen transgenes produce tumors and cardiac arrhythmias in mice. Science 239:1029–1033

Hamill OP, Marty A, Neher E et al (1981) Improved patch-clamp techniques for high-resolution current recording from cells and cell-free membrane patches. Pflugers Arch 391:85–100

Hannon GJ (2002) RNA interference. Nature 418:244–251

Honjo H, Boyett MR, Kodama I et al (1996) Correlation between electrical activity and the size of rabbit sino-atrial node cells. J Physiol 496:795–808

Jones EM, Roti Roti EC, Wang J et al (2004) Cardiac I_{Kr} channels minimally comprise hERG 1a and 1b subunits. J Biol Chem 279:44690–44694

Lees-Miller JP, Kondo C, Wang L et al (1997) Electrophysiological characterization of an alternatively processed ERG K^+ channel in mouse and human hearts. Circ Res 81:719–726

Lei M, Honjo H, Kodama I et al (2001) Heterogeneous expression of the delayed-rectifier K^+ currents $i_{K,r}$ and $i_{K,s}$ in rabbit sinoatrial node cells. J Physiol 535:703–714

Liu DW, Antzelevitch C (1995) Characteristics of the delayed rectifier current (I_{Kr} and I_{Ks}) in canine ventricular epicardial, midmyocardial, and endocardial myocytes. A weaker I_{Ks} contributes to the longer action potential of the M cell. Circ Res 76:351–365

Liu Y, Taffet SM, Anumonwo JM et al (1994) Characterization of an E4031-sensitive potassium current in quiescent AT-1 cells. J Cardiovasc Electrophysiol 5:1017–1030

Liu S, Rasmusson RL, Campbell DL et al (1996) Activation and inactivation kinetics of an E-4031-sensitive current from single ferret atrial myocytes. Biophys J 70:2704–2715

London B, Trudeau MC, Newton KP et al (1997) Two isoforms of the mouse *ether-a-go-go*-related gene coassemble to form channels with properties similar to the rapidly activating component of the cardiac delayed rectifier K^+ current. Circ Res 81:870–878

Matsuura H, Ehara T, Ding WG et al (2002) Rapidly and slowly activating components of delayed rectifier K^+ current in guinea-pig sino-atrial node pacemaker cells. J Physiol 540:815–830

McDonald TV, Yu Z, Ming Z et al (1997) A minK-HERG complex regulates the cardiac potassium current I_{Kr}. Nature 388:289–292

McWhinney CD, Hansen C, Robishaw JD (2000) Alpha-1 adrenergic signaling in a cardiac murine atrial myocyte (HL-1) cell line. Mol Cell Biochem 214:111–119

Morais Cabral JH, Lee A, Cohen SL et al (1998) Crystal structure and functional analysis of the HERG potassium channel N-terminus: a eukaryotic PAS domain. Cell 95:649–655

Neilan CL, Kenyon E, Kovach MA et al (2000) An immortalized myocyte cell line, HL-1, expresses a functional δ-opioid receptor. J Mol Cell Cardiol 32:2187–2193

Niwa N, Yasui K, Opthof T et al (2004) $Ca_v3.2$ subunit underlies the functional T-type Ca^{2+} channel in murine hearts during the embryonic period. Am J Physiol 286:H2257–H2263

Ono K, Ito H (1995) Role of rapidly activating delayed rectifier K^+ current in sinoatrial node pacemaker activity. Am J Physiol 269:H453–H462

Phartiyal P, Jones EMC, Robertson GA (2007) Heteromeric assembly of human ether-à-go-go-related gene (hERG) 1a/1b channels occurs cotransfectionally via N-terminal interactions. J Biol Chem 282:9874–9882

Pond AL, Scheve BK, Benedict AT et al (2000) Expression of distinct ERG proteins in rat, mouse, and human heart. Relation to functional I_{Kr} channels. J Biol Chem 275:5997–6006

Roden DM, Lazzara R, Rosen M et al (1996) Multiple mechanisms in the long-QT syndrome. Current knowledge, gaps, and future directions. The SADS Foundation Task Force on LQTS. Circulation 94:1996–2012

Sale H, Wang J, O'Hara TJ et al (2008) Physiological properties of hERG 1a/1b heteromeric currents and a hERG 1b-specific mutation associated with long-QT syndrome. Circ Res 103: e81–e95

Sanguinetti MC, Jurkiewicz NK (1990) Two components of cardiac delayed rectifier K^+ current. Differential sensitivity to block by class III antiarrhythmic agents. J Gen Physiol 96:195–215

Sanguinetti MC, Jiang C, Curran ME et al (1995) A mechanistic link between an inherited and an acquired cardiac arrhythmia: *HERG* encodes the I_{Kr} potassium channel. Cell 81:299–307

Sartiani L, Bochet P, Cerbai E et al (2002) Functional expression of the hyperpolarization-activated, non-selective cation current I_f in immortalized HL-1 cardiomyocytes. J Physiol 545:81–92

Shibasaki T (1987) Conductance and kinetics of delayed rectifier potassium channels in nodal cells of the rabbit heart. J Physiol 387:227–250

Smith PL, Baukrowitz T, Yellen G (1996) The inward rectification mechanism of the HERG cardiac potassium channel. Nature 379:833–836

Trudeau MC, Warmke JW, Ganetzky B et al (1995) HERG, a human inward rectifier in the voltage-gated potassium channel family. Science 269:92–95

Wang L, Duff HJ (1996) Identification and characteristics of delayed rectifier K^+ current in fetal mouse ventricular myocytes. Am J Physiol 270:H2088–H2093

Wang L, Feng ZP, Kondo CS et al (1996) Developmental changes in the delayed rectifier K^+ channels in mouse heart. Circ Res 79:79–85

Weerapura M, Nattel S, Chartier D et al (2002) A comparison of currents carried by HERG, with and without coexpression of MiRP1, and the native rapid delayed rectifier current. Is MiRP1 the missing link? J Physiol 540:15–27

White SM, Constantin PE, Claycomb WC (2004) Cardiac physiology at the cellular level: use of cultured HL-1 cardiomyocytes for studies of cardiac muscle cell structure and function. Am J Physiol 286:H823–H829

Xia M, Salata JJ, Figueroa DJ et al (2004) Functional expression of L- and T-type Ca^{2+} channels in murine HL-1 cells. J Mol Cell Cardiol 36:111–119

Yang T, Roden DM (1996) Extracellular potassium modulation of drug block of I_{Kr}. Implications for torsade de pointes and reverse use-dependence. Circulation 93:407–411

Yang T, Wathen MS, Felipe A et al (1994) K^+ currents and K^+ channel mRNA in cultured atrial cardiac myocytes (AT-1 cells). Circ Res 75:870–878

Yang T, Kupershmidt S, Roden DM (1995) Anti-minK antisense decreases the amplitude of the rapidly activating cardiac delayed rectifier K^+ current. Circ Res 77:1246–1253

Yang T, Snyders DJ, Roden DM (1997) Rapid inactivation determines the rectification and $[K^+]_o$ dependence of the rapid component of the delayed rectifier K^+ current in cardiac cells. Circ Res 80:782–789

Yasui K, Liu W, Opthof T et al (2001) I_f current and spontaneous activity in mouse embryonic ventricular myocytes. Circ Res 88:536–542

Zankov DP, Yoshida H, Tsuji K et al (2009) Adrenergic regulation of the rapid component of delayed rectifier K^+ current: implications for arrhythmogenesis in LQT2 patients. Heart Rhythm 6:1038–1046

Zhou Z, Gong Q, Ye B et al (1998) Properties of HERG channels stably expressed in HEK 293 cells studied at physiological temperature. Biophys J 74:230–241

A family of hereditary long QT syndrome caused by Q738X HERG mutation

Shioto Yasuda [a], Shin-ichi Hiramatsu [a], Keita Odashiro [a], Toru Maruyama [a,*], Keiko Tsuji [b], Minoru Horie [b]

[a] The Department of Medicine and Biosystemic Science, Kyushu University Graduate School of Medical Sciences, Fukuoka 812-8582, Japan
[b] Department of Cardiovascular and Respiratory Medicine, Shiga University of Medical Science, Otsu 520-2192, Japan

Received 5 August 2008; accepted 6 December 2008
Available online 21 January 2009

Keywords: Genetic mutation; HERG channel; Long QT syndrome; Torsade de Pointes

Dear Sir,

Hereditary long QT syndromes (LQTS) are autosomal dominant familial disorders characterized by impaired cardiac repolarization and QT prolongation leading to Torsade de Pointes (TdP). Among them, type 2 LQTS (LQT2) is caused by mutations in the human ether a-go-go related gene (HERG) channel gene [1]. Typical ECG manifestation of LQT2 is prolonged QT interval with flat T wave, and TdP is likely to occur at rest by emotional stress evoked by auditory stimuli [2]. Here, we report a small family of hereditary LQT2 caused by a novel HERG mutation, showing a wide variety of ECG phenotypes among family members under the common single nucleotide mutation (c.C2212T and p.Q738X).

A 42-year-old female referred to our hospital due to syncope. ECG showed an increase in QT interval and flat T wave (Fig. 1A). Ambulatory monitoring demonstrated lack of QT shortening under an increase in heart rate during walking. Thereafter, heart rate decreased and QT prolonged further causing short segment of TdP in the morning (Fig. 1B). Although lack of rate adaptation in QT interval was partly restored by propranolol (20 mg/day), she was not tolerant to oral propranolol due to fatigue. Her father underwent pacemaker implantation for back-up pacing against advanced atrioventricular (AV) block, when he was 38-year-old. Thereafter, he exhibited persistent atrial flutter with QT interval of 420 ms at age of 43-year-old (Fig. 1C). Her second daughter is now 10-year-old, and shows long QT interval (480 ms) with broad-based, sharp T wave (Fig. 1D).

Suspecting genetic disorder causing familial LQTS, DNA isolation and mutation analysis were performed as introduced elsewhere [3] after obtaining written informed consent. Gene analysis revealed that the proband, her father and daughter commonly showed a single nucleotide HERG mutation of c.C2212T in a heterozygous manner (Fig. 2) causing a stop codon at 738 (p.Q738X). No other mutations were found in LQTS-associated genes such as KCNQ1, KCNE1, KCNE2, KCNJ2 and SCN5A. By informing of the risk of sudden death, she underwent implantation of dual chamber ICD. After the implantation, she has experienced no syncope without ICD discharge. Her daughter is asymptomatic under careful observation without device or medication.

It is of great interest that ECG phenotypes in this LQT2 family showed a considerable variation, i.e., the proband showed ECG compatible to LQT2 (Fig. 1A) and no rate adaptation of QT interval, postexercise QT prolongation and subsequent TdP (Fig. 1B), which is observed in 13% of overall cardiac events in LQT2 patients [2], whereas her father had advanced AV block and subsequent persistent atrial flutter with normal QT interval (Fig. 1C), and her daughter showed long QT interval with broad-based, tall T wave (Fig. 1D). Reportedly, various kinds of atrial tachyarrhythmias are associated with LQTS [4]. T wave morphology recorded in her daughter is observed mainly in LQT1 but in 32% of LQT2 [3].

HERG K channel conducts rapid component of delayed rectifier K current (I_{Kr}), which is essential for normal cardiac repolarization. To our knowledge, Q738X HERG mutation has not been registered in HERG-related Online Mendelian Inheritance in Man (OMIM; http://pc4.fsm.it:81/cardmoc). The Q738X product results in the deletion of 86% of the C-terminus. Since a single HERG channel protein

* Corresponding author. Tel.: +81 92 642 5235 (direct line); fax: +81 92 642 5247.
E-mail address: maruyama@ihs.kyushu-u.ac.jp (T. Maruyama).

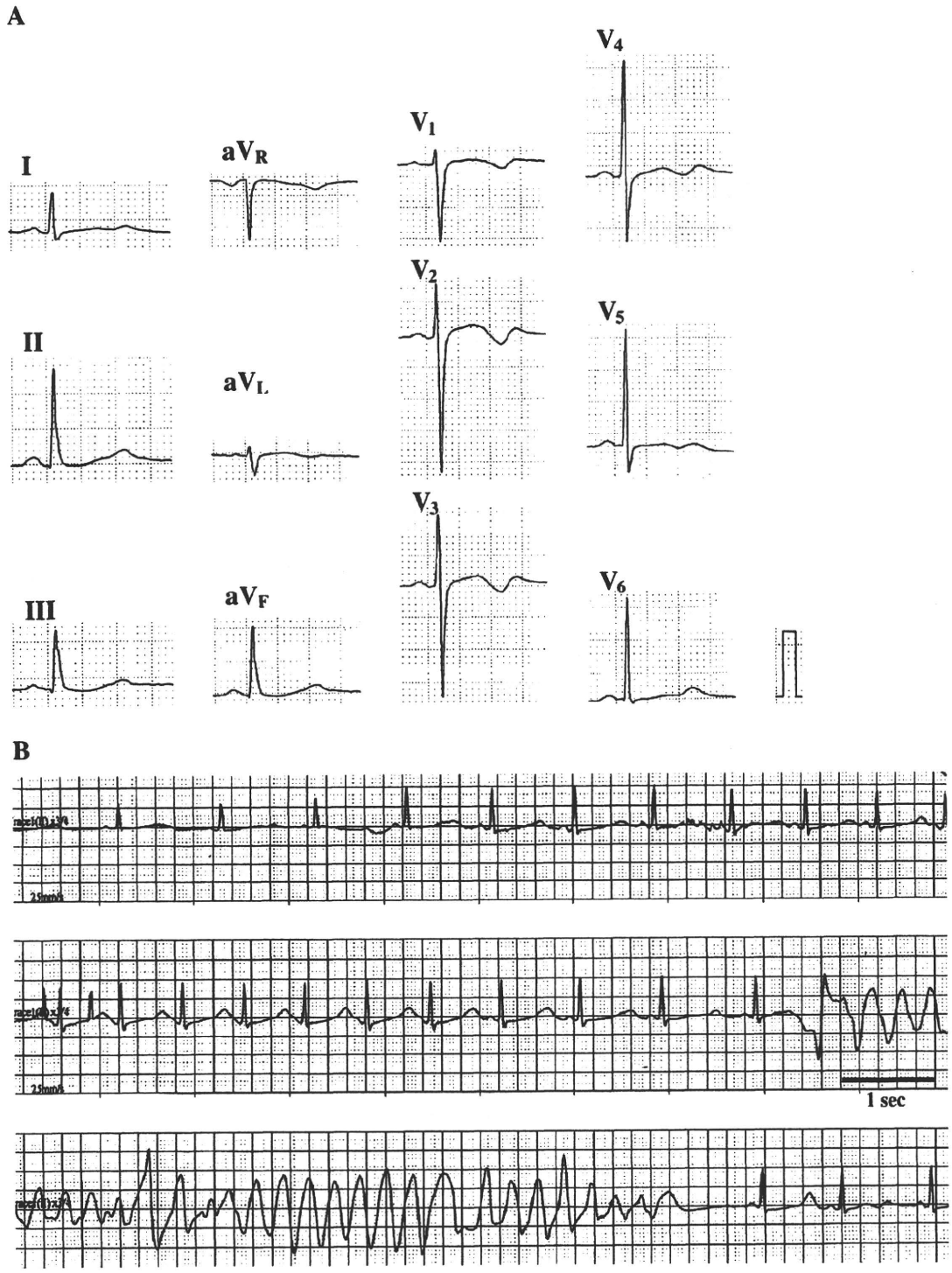

Fig. 1. A; Standard ECG of proband showed QT interval of 520 ms and flat T wave. B; Ambulatory monitoring demonstrated lack of rate adaptation in QT interval and subsequent Torsades de Pointes in the morning. C; Her father showed atrial flutter with ventricular pacing. D; Her daughter exhibited long QT (480 ms) with broad-based, sharp T wave.

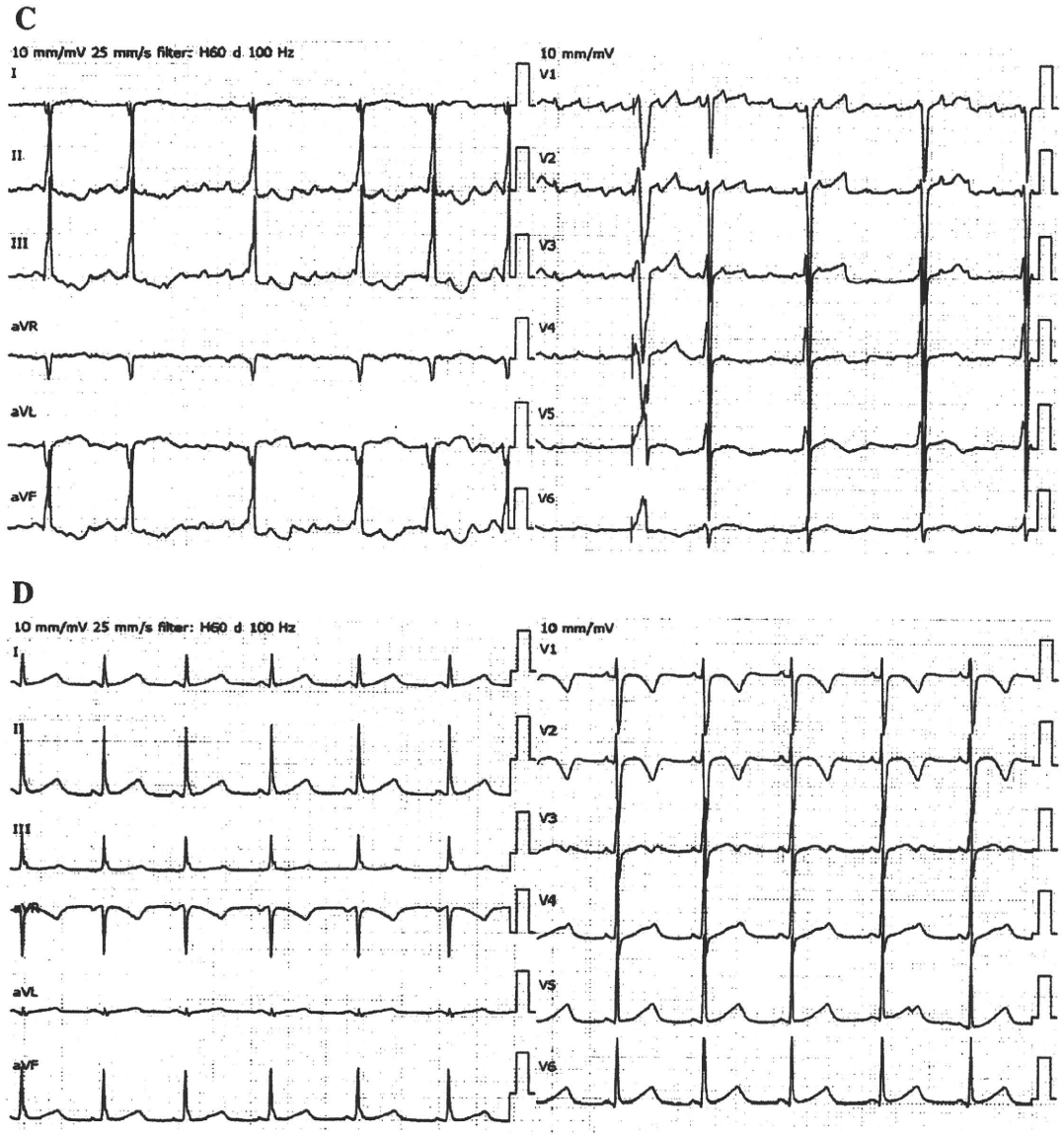

Fig. 1 (*continued*).

consists of four α-subunits, the truncated subunit based on Q738X would hinder the normal assembly of healthy subunits and therefore exerting a dominant negative suppression effects. Although an *in vitro* expression study was not performed, these effects are considered to suppress I_{Kr} profoundly and yield the LQT2 phenotypes in the proband and her family. However, the nonsense Q738X mutation may cause a nonsense-mediated mRNA decay (NMD) and avoid dominant negative suppressions as a post-transcriptional control. The severity of the phenotypes would therefore differ depending on the degree of NMD level [5]. This may be a main reason for varied QT intervals and T wave morphologies in this relatively small LQT2 family.

The authors of this manuscript have certified that they comply with the Principles of Ethical Publishing in the International Journal of Cardiology [6].

References

[1] Curran ME, Splawski I, Timothy KW, Vincent GM, Green ED, Keating MT. A molecular basis for cardiac arrhythmia: HERG mutations cause long QT syndrome. Cell 1995;80:795–803.

[2] Schwartz PJ, Priori SG, Spazzolini C, et al. Genotype–phenotype correlation in the long-QT syndrome. Circulation 2001;103:89–95.

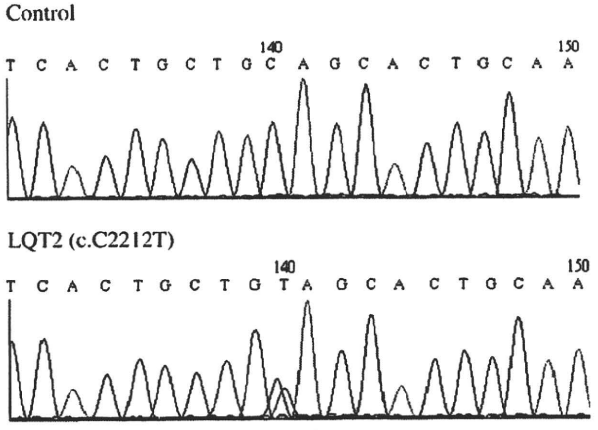

Fig. 2. Mutation analysis of family members. Chromatograms showed a common single nucleotide mutation of c.C2212T, causing amino acid sequence of p.Q738X.

[3] Takenaka K, Ai T, Shimizu W, et al. Exercise stress test amplifies genotype–phenotype correlation in the LOT1 and LQT2 forms of the long-QT syndrome. Circulation 2003;107:838–44.
[4] Kirchhof P, Eckardt L, Franz MR, et al. Prolonged atrial action potential durations and polymorphic atrial tachyarrhythmias in patients with long QT syndrome. J Cardiovasc Electrophysiol 2003;14:1027–33.
[5] Gong Q, Zhang L, Vincent GM, Horne BD, Zhou Z. Nonsense mutations in hERG cause a decrease in mutant mRNA transcripts by nonsense-mediated mRNA decay in human long-QT syndrome. Circulation 2007;116:17–24.
[6] Coats AJ. Ethical authorship and publishing. Int J Cardiol 2009;131: 149–50.

0167-5273/$ - see front matter
doi:10.1016/j.ijcard.2008.12.053

Atrial natriuretic peptide polymorphisms, hydrochlorothiazide and urinary potassium excretion

Stefan Viktor Vormfelde [a,*], Mohammad Reza Toliat [b], Peter Nürnberg [b], Jürgen Brockmöller [a]

[a] *Department of Clinical Pharmacology, University Medical Center, Robert-Koch-Str. 40, 37075 Göttingen, Germany*
[b] *Cologne Center for Genomics (CCG) and Institute for Genetics, University of Cologne, Zuelpicher Straße 47, 50674 Köln, Germany*

Received 6 August 2008; accepted 6 December 2008
Available online 11 January 2009

Keywords: Atrial natriuretic peptide; Genetic polymorphism; Thiazide diuretic; Hydrochlorothiazide; Antihypertensive therapy; Potassium

NPPA disruption goes with salt-sensitive hypertension in mice [1]. In humans, the methionine32 allele of Val32Met (G664A, rs5063) has been associated with low circulating proANP levels [2]. Both methionine32 and the arginine152 allele of the Ter152Arg polymorphism (T2238C, rs5065) have been associated with hypertension or hypertension-related disease (overview in [3]). In conclusion, both variant alleles are supposed to be low functional alleles compared to the respective wild-type alleles. Now, in the ALLHAT study, coronary heart disease outcome tended better or was significantly better in carriers of the variant alleles [3]. In contrast, the overall survival tended lower in these subjects. We explored a potential association of the *NPPA* polymorphisms with diuretic effects of another thiazide diuretic, hydrochlorothiazide, in a single-dose cross-over study with 25 and 100 mg hydrochlorothiazide in 103 healthy, normotensive volunteers.

The study was approved by the Ethics committee of the University of Göttingen; all participants provided written informed consent. The participants were 103 normotensive, healthy, male Caucasian volunteers aged between 18 and

* Corresponding author. Tel.: +49 551 399651; fax: +49 551 12767.
E-mail address: svormfe@gwdg.de (S.V. Vormfelde).

The combination of STFT configuration variables that achieved the highest TDA (86%) was improved in regard to that reported by Barbosa et al. [7]. This indicated that, a larger time window and a larger step between successive time samples best discriminated both groups. Thus, in STFT-derived spectral turbulence analysis, it is possible to consider that the fluctuations of electrical transients are more appropriately defined when analyzing time window is large enough and sample times are apart from each other.

Short and medium term reproducibility studies of spectral turbulence variables have already been carried out elsewhere, to validate present results [8].

In conclusion, spectral resolution affects diagnostic accuracy in SAECG STFT-derived spectral turbulence analysis. An optimal configuration of STFT creation variable combines: 40 ms time window width, 512 points *zero-padding*, 4 ms time displacement steps, −2 ms displacement from starting position. Diagnostic criterion of two abnormal spectral turbulence related variables among four possible, along with STFT configuration that assesses 40 ms time window in the ventricular activation are the optimal configuration allowing for appropriate discrimination between Control and SMVT groups.

The study was supported by Brazilian National Research Council (CNPq).

The authors of this manuscript have certified that they comply with the Principles of Ethical Publishing in the International Journal of Cardiology [9].

References

[1] Ahuja RK, Turitto G, Ibrahim B, Caref EB, El-Sherif N. Combined time-domain and spectral turbulence analysis of the signal-averaged ECG improves its predictive accuracy in postinfarction patients. J Electrocardiol 1994;27(1):202–6.
[2] Vásquez R, Caref EB, Torres F, Reina M, Espina A, El-Sherif N. Improved diagnostic value of combined time and frequency domain analysis of the signal-averaged electrocardiogram after myocardial infarction. JACC 1999;33(2):385–94.
[3] Kelen GJ, Henkin R, Starr A, Caref EB, Bloomfield D, El-Sherif N. Spectral turbulence analysis of the signal-averaged electrocardiogram and its predictive accuracy for inducible sustained monomorphic ventricular tachycardia. Am J Cardiol 1991;67(11):965–75.
[4] Benchimol-Barbosa PR, de Souza Bomfim A, Barbosa EC, et al. Spectral turbulence analysis of the signal-averaged electrocardiogram of the atrial activation as predictor of recurrence of idiopathic and persistent atrial fibrillation. Int J Cardiol 2006;107(3):307–16.
[5] Benchimol-Barbosa PR, Barbosa-Filho J, de Sá CA, Nadal J. Reduction of electromyographic noise in the signal-averaged electrocardiogram by spectral decomposition. IEEE Trans Biomed Eng 2003;50(1):114–7.
[6] Benchimol-Barbosa PR, Muniz RT. Ventricular late potential duration correlates to the time of onset of electrical transients during ventricular activation in subjects post-acute myocardial infarction. Int J Cardiol 2008;129(2):285–7.
[7] Barbosa EC, Benchimol-Barbosa PR, Ginefra P, Albanesi FM. O eletrocardiograma de alta resolução no domínio da frequência. Utilização de correlação espectral para identificação de pacientes com taquicardia ventricular monomórfica sustentada [In portuguese]. Arq Bras Cardiol 1998;71(4):595–9.
[8] Benchimol-Barbosa PR, Bomfim AS, Barbosa EC, Boghossian S, Barbosa-Filho J, Albanesi-Filho FM. Reproducibility of spectral turbulence measurements post ST elevation. Cardiorhythm, 2007, Hong Kong. Europace. Hong Kong: Oxford University Press; 2007. 9:66.
[9] Coats AJ. Ethical authorship and publishing. Int J Cardiol 2009;131:149–50.

0167-5273/$ – see front matter
doi:10.1016/j.ijcard.2009.04.013

A novel SCN5A mutation associated with the linker between III and IV domains of $Na_v1.5$ in a neonate with fatal long QT syndrome

Kenichiro Yamamura [a,*], Jun Muneuchi [a], Kiyoshi Uike [a], Kazuyuki Ikeda [a], Hirosuke Inoue [a], Yasushi Takahata [a], Yuichi Shiokawa [b], Yukako Yoshikane [c], Takeru Makiyama [d], Minoru Horie [e], Toshiro Hara [a]

[a] *Department of Pediatrics, Graduate School of Medical Sciences, Kyushu University, Japan*
[b] *Department of Cardiovascular Surgery, Graduate School of Medical Sciences, Kyushu University, Japan*
[c] *Department of Pediatrics, Fukuoka University Hospital, Japan*
[d] *Department of Cardiovascular Medicine, Graduate School of Medicine, Kyoto University, Japan*
[e] *Department of Cardiovascular and Respiratory Medicine, Shiga University of Medical Science, Japan*

ARTICLE INFO

Article history:
Received 8 April 2009
Accepted 11 April 2009
Available online 6 May 2009

Keywords:
Long QT syndrome
Fetal arrhythmia
SCN5A
Linker of III–IV domains

* Corresponding author. Department of Pediatrics, Graduate School of Medical Sciences, Kyushu University, 3-1-1, Maidashi, Higashi-ku, Fukuoka, 812-8582, Japan. Tel.: +81 92 642 5421; fax: +81 92 642 5435.
E-mail address: yamamura@pediatr.med.kyushu-u.ac.jp (K. Yamamura).

Congenital long QT syndrome (LQTS) is a genetically heterogeneous disorder caused by mutations in cardiac ion channels [1]. Patients with LQTS are predisposed to syncope, life-threatening arrhythmias and sudden death due to delayed ventricular repolarization. Clinical manifestations of LQTS are variable according to gender, age and genetic backgrounds. LQTS concurrent with lower heart rate or atrioventricular block is rare but fatal, which usually manifests itself before birth or during the neonatal period.

The mutation in *SCN5A*, which encodes the alpha subunit of cardiac voltage-gated sodium channel ($Na_v1.5$), is responsible for LQTS type3 (LQT3). As more than 150 mutations in *SCN5A* have been reported [2], several types of mutations such as P1332L and F1473C are associated with intrauterine and neonatal manifestations of LQT3 with the higher mortality [3].

We here present a notable case of a neonate with fatal LQT3 who pre- and postnatally developed atrioventricular block and ventricular tachycardia (VT). Genetic analysis demonstrated a novel *de novo*

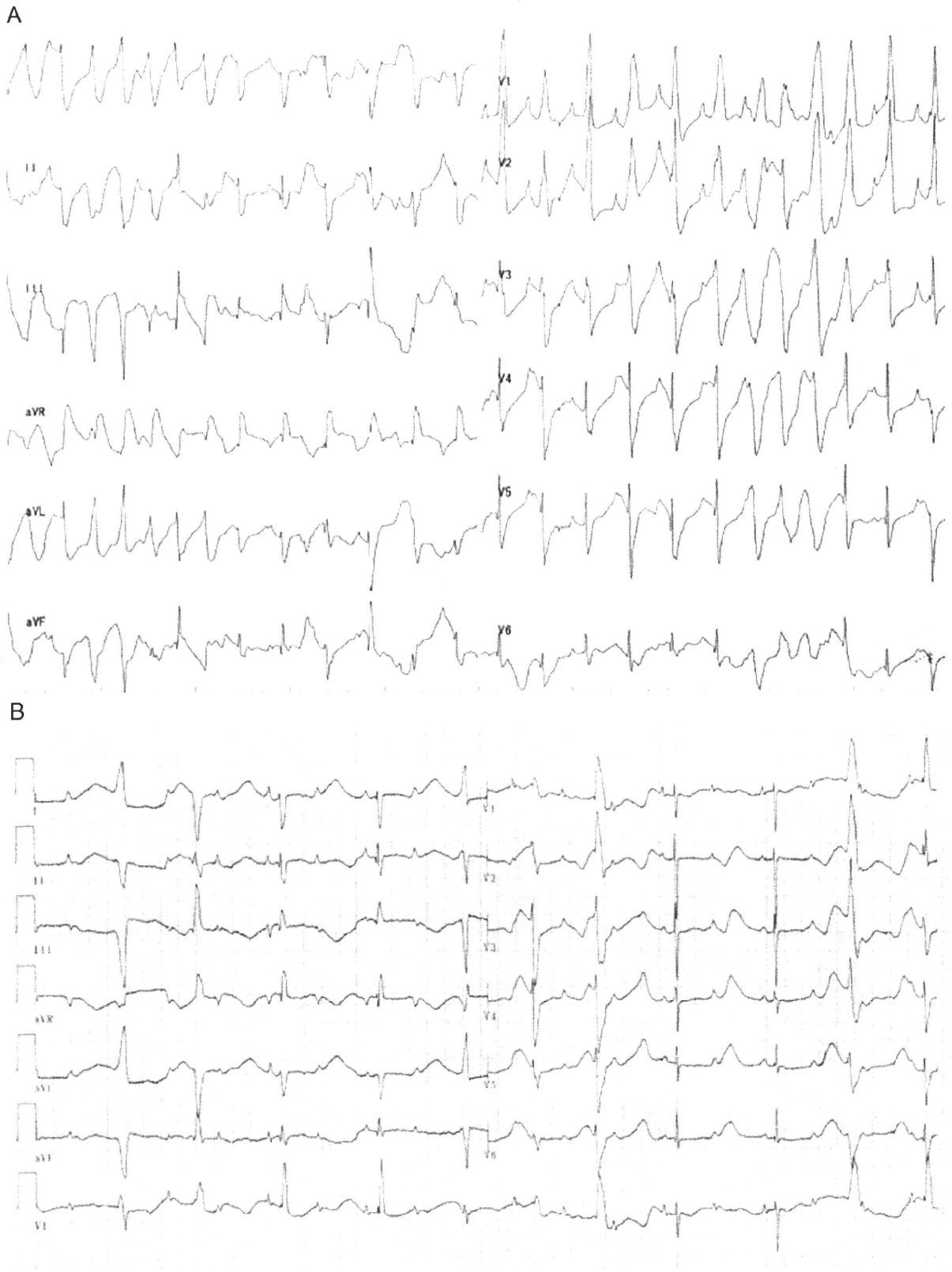

Fig. 1. Twelve-lead electrocardiogram at admission (A), and after administration of amiodarone (B). Paper speed 25 mm/s; 10 mm/1 mV. A, Polymorphic ventricular tachycardia. B, 2:1 Atrioventricular block (HR 56 bpm, atrial rate 112 bpm) due to extremely prolonged corrected QT interval (as long as 860 ms).

heterozygous mutation in SCN5A associated with the linker between III and IV domains of $Na_v1.5$.

A male newborn weighing 2334 g was delivered at 37 weeks of gestation by caesarean section because prenatal ultrasound demonstrated fetal hydrops with atrioventricular block, incessant ventricular tachycardia and decreased ventricular function. There was no maternal obstetrical or medical history. As he had poor perfusion and respiratory insufficiency, assisted ventilation and administration of dobutamine were started. Irregular and weak pulsation was noted. Chest X-ray showed that cardiothoracic ratio was 67%. Echocardiogram showed dilated left ventricle, decreased left ventricular ejection fraction (23%) and significant pericardial effusion. Electrocardiogram (ECG) demonstrated 2:1 atrioventricular block and polymorphic ventricular tachycardia (VT) (Fig. 1A). VT was refractory to intravenous administration of magnesium (50 mg/kg) and lidocaine (3 mg/kg). Although prenatal ultrasound raised the suspicion of LQTS, a definitive diagnosis was not made. To improve the circulatory instability, the patient was given a test dose of intravenous amiodarone (5 mg/kg) which resulted in termination of VT. ECG in sinus rhythm showed 2:1 atrioventricular block (atrial rate of 112 bpm and ventricular rate of 56 bpm) with an excessive QT prolongation (corrected QT interval, 860 ms) and late-appearing T wave (Fig. 1B). However, after a few minutes, ECG demonstrated VT again with following circulatory instability. Further administration of lidocaine, beta-blocker and amiodarone was ineffective. Cardiac pacing was intended to increase heart rate, but in failure. In spite of repetitive cardioversion and chest compressions, he died 18 h after birth. Autopsy was not performed.

There was no family history of prolonged QT interval, syncope, or sudden death. Both parents had screening electrocardiograms with normal QT intervals. There was no sibling.

Genetic DNA was extracted from venous EDTA blood of the present patient and his parents by standard procedure. Because of the ECG phenotype, all coding regions of *SCN5A* were first sequenced directly. Abnormal conformers were amplified by polymerase chain reaction, and sequencing was performed on an ABI PRISM 3100 DNA sequencer (Applied Biosystems, Foster City, California). A heterozygous deletion of TTC at nucleotide position 4456–4458 in exon 26 was detected in the present patient (Fig. 2A). No other mutations were detected in *SCN5A*. We have also found no mutation in *KVLQT1* and *HERG* genes. This nucleotide deletion was predicted to cause an amino deletion of phenylalanine at 1486 (F1486del, III–IV linker of $Na_v1.5$). In a large control population, this mutation was absent, making it less likely that it was a rare polymorphism. Since the mutation was not identified in both parents, we considered it to be a *de novo* mutation.

We present a notable case of a neonate with fatal LQT3 who had a novel *SCN5A* mutation associated with the III–IV linker domain of $Na_v1.5$. In the present case, the corrected QT interval (860 ms) was the longest among the LQTS patients in the previous reports [1,3,4]. To our knowledge, there were only seven case reports of fetal or neonatal onset LQT3 with *SCN5A* mutations [3–9]. A neonate with F1473C mutation in III–IV linker also presented the second longest corrected QT interval (825 ms) which suggested the III–IV linker plays an important role to regulate the sodium channel function [3].

Previous reports indicate that the intracellular loop between domains III and IV of $Na_v1.5$ forms the inactivation gate [10]. A three-residue hydrophobic motif (IFM: 1485I-1486F-1487M) is an essential structural feature of the gate and serves as an inactivation particle that binds within the pore. F1486del mutation identified in the present case resulted in a deletion of the center of this hydrophobic amino acid cluster (Fig. 2B). We considered that F1486del mutation in *SCN5A* is critical to inactivate $Na_v1.5$.

The use of amiodarone was very controversial. ECG after birth was so complicated that we were unable to measure the QT interval exactly. Intravenous amiodarone might have some adverse effects, although it was described that intravenous administration of amiodarone had only little effect to QT intervals [11]. In the present case, the administration of lidocaine was unable to cease VT, although previous reports suggested the efficacy of lidocaine or mexiletine in LQT3 neonates with *SCN5A* mutations. Unfortunately, intravenous mexiletine was not available in our institute. Ruan et al. reported that the response to mexiletine varied among patients harboring different mutations in *SCN5A* [12]. It is assumed that the mutation in III–IV

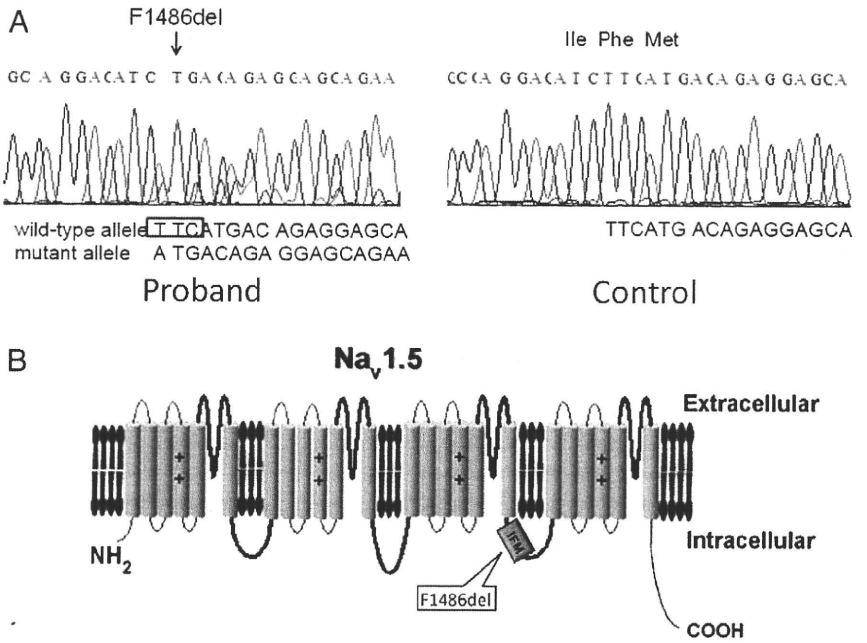

Fig. 2. A, The sequence analysis of exon 26 in *SCN5A*. A heterozygous deletion of TTC at nucleotide position 4456–4458 was detected in the proband. This nucleotide deletion was predicted to cause an amino deletion of phenylalanine at 1486 (F1486del). B, Diagrammatic representation of the human cardiac sodium channel displaying the location of the mutation identified in the present case. F1486del mutation resulted in a deletion of the amino acid in the center of IFM motif.

linker may be associated with the resistance to sodium channel blockers such as lidocaine or mexiletine.

In summary, we identified a novel *de novo SCN5A* mutation in a neonate with extremely prolonged QT interval resulting in cardiac death in the first day of life. This mutation is associated with the IFM motif in the linker between III and IV domains of $Na_v1.5$, which serves as an inactivation particle binding within the pore of sodium channels. This report demonstrates an interesting relationship between clinical phenotype and the location of the mutation and supported the importance of genetic analysis and tailored therapy in neonatal LQTS.

The authors of this manuscript have certified that they comply with the Principles of Ethical Publishing in the International Journal of Cardiology [13].

References

[1] Goldenberg I, Moss AJ. Long QT syndrome. J Am Coll Cardiol Jun 17 2008;51(24):2291–300.
[2] Remme CA, Wilde AA, Bezzina CR. Cardiac sodium channel overlap syndromes: different faces of SCN5A mutations. Trends Cardiovasc Med Apr 2008;18(3):78–87.
[3] Bankston JR, Yue M, Chung W, et al. A novel and lethal de novo LQT-3 mutation in a newborn with distinct molecular pharmacology and therapeutic response. PLoS ONE 2007;2(12):e1258.
[4] Chang CC, Acharfi S, Wu MH, et al. A novel SCN5A mutation manifests as a malignant form of long QT syndrome with perinatal onset of tachycardia/bradycardia. Cardiovasc Res Nov 1 2004;64(2):268–78.
[5] Wedekind H, Smits JP, Schulze-Bahr E, et al. De novo mutation in the SCN5A gene associated with early onset of sudden infant death. Circulation Sep 4 2001;104(10):1158–64.
[6] Schulze-Bahr E, Fenge H, Etzrodt D, et al. Long QT syndrome and life threatening arrhythmia in a newborn: molecular diagnosis and treatment response. Heart Jan 2004;90(1):13–6.
[7] Miura M, Yamagishi H, Morikawa Y, Matsuoka R. Congenital long QT syndrome and 2:1 atrioventricular block with a mutation of the SCN5A gene. Pediatr Cardiol Jan–Feb 2003;24(1):70–2.
[8] Ten Harkel AD, Witsenburg M, de Jong PL, Jordaens L, Wijman M, Wilde AA. Efficacy of an implantable cardioverter–defibrillator in a neonate with LQT3 associated arrhythmias. Europace Jan 2005;7(1):77–84.
[9] Miller TE, Estrella E, Myerburg RJ, et al. Recurrent third-trimester fetal loss and maternal mosaicism for long-QT syndrome. Circulation Jun 22 2004;109(24):3029–34.
[10] McPhee JC, Ragsdale DS, Scheuer T, Catterall WA. A critical role for transmembrane segment IVS6 of the sodium channel alpha subunit in fast inactivation. J Biol Chem May 19 1995;270(20):12025–34.
[11] Kodama I, Kamiya K, Toyama J. Cellular electropharmacology of amiodarone. Cardiovasc Res Jul 1997;35(1):13–29.
[12] Ruan Y, Liu N, Bloise R, Napolitano C, Priori SG. Gating properties of SCN5A mutations and the response to mexiletine in long-QT syndrome type 3 patients. Circulation Sep 4 2007;116(10):1137–44.
[13] Coats AJ. Ethical authorship and publishing. Int J Cardiol 2009;131:149–50.

0167-5273/$ – see front matter
doi:10.1016/j.ijcard.2009.04.023

Predicting prognosis in patients with Chagas disease: Why are the results of various studies so different?

Anis Rassi Jr.*, Anis Rassi

Division of Cardiology, Anis Rassi Hospital, Goiânia, Brazil

ARTICLE INFO

Article history:
Received 14 April 2009
Accepted 23 April 2009
Available online 9 May 2009

Keywords:
Chagas disease
Prognosis
Risk factors
Mortality
Risk stratification
Prediction

The article by Gonçalves and colleagues [1] describes predictors of death among patients with chronic Chagas disease living in an endemic area in Minas Gerais (Brazil). In a retrospective analysis of 120/187 (64.2%) patients with the indeterminate or cardiac form of the disease who could be followed for a mean of 18.5 years, the investigators observed 42 deaths (21 of cardiovascular origin, 7 sudden and 14 due to other causes). Using the Cox regression model, 20 dichotomous demographic, behavioral, clinical and electrocardiographic variables were initially evaluated to calculate the proportional mortality risk from all causes, cardiovascular causes, and sudden death, relative to each variable (univariate analysis). Of these, 12 variables presented statistical significance ($p<0.05$) and were entered into the multivariate model. For all-cause mortality, 5 variables retained independent prognostic significance: age≥39 years (HR 2.19; 95% CI 1.08–4.43; $p=0.028$), black skin colour (HR 6.09; 95% CI 1.23–30.19; $p=0.026$), complete right bundle branch block associated with left anterior fascicular block (HR 34.61; 95% CI 4.32–276.98; $p=0.0008$), complete left bundle branch block (HR 654.92; 95% CI 22.78–18,823.27; $p=0.0002$) and polymorphic ventricular extrasystoles on the 12-lead ECG (HR 8.08 billion; 95% CI 23.76 million to >10E12; $p<0.001$). For cardiovascular mortality, 5 variables were found to be independent prognostic markers in the multivariate analysis: black skin colour (HR 17.72; 95% CI 1.81–172.93; $p=0.013$), complete right bundle branch block associated with left anterior fascicular block (HR 22.86; 95% CI 1.26–413.42; $p=0.034$), complete left bundle branch block (HR 143.73; 95% CI 1.29–15,952.01; $p=0.038$), polymorphic ventricular extrasystoles (HR 921,062.88; 95% CI 234.53–3.62 billion; $p=0.001$) and PR interval ≥0.16 s (HR 9.00; 95% CI 1.98–40.87; $p=0.004$). For sudden death, 4 variables were identified: complete right bundle branch block (HR 233.09; 95% CI 8.57–6339.89; $p=0.001$), left anterior fascicular block (HR 11,490.43; 95% CI 155.24–850,486.33; $p<0.001$), complete left bundle branch block (HR 54,679.94; 95% CI 42.40–70.51 million; $p=0.002$) and polymorphic ventricular extrasystoles (HR 4.04 billion; 95% CI 245,345.20 to >10E12; $p<0.001$).

This investigation reports some unusual findings that merit further discussion. In contrast to other studies, black skin colour, PR interval ≥0.16 s and complete right bundle branch block (amongst others

* Corresponding author. Tel.: +55 62 32279105; fax: +55 62 3227 9311.
E-mail address: arassijr@terra.com.br (A. Rassi Jr.).

Editorial

Bi-directional Ventricular Tachycardia Revised

The nomenclature of bi-directional ventricular tachycardia (BVT) apparently came from its peculiar ECG morphology showing QRS complexes alternatively changing the frontal axis during ventricular tachycardia. Clinically, BVT was reported as early as 1954 and most often seen in digitalis intoxication. The term BVT was therefore not based on the functional mechanism. However, the molecular basis for two types of inherited ion channel diseases that commonly show BVT has recently been partially elucidated. Accordingly, the concept in regard to BVT may require some reconsideration.

Two other pathological conditions with frequently-observed BVT are Andersen-Tawil syndrome (ATS) and catecholaminergic polymorphic ventricular tachycardia (CPVT). **Figure 1** depicts a 12-leads ECG recorded from a case of genotyped ATS. The patient was initially diagnosed with long QT syndrome since her ECG showed a markedly prolonged QT interval and lacked two other clinical hallmarks of ATS: periodic paralysis and dysmorphic features. Cardiac phenotypes in ATS are characterized by prolongation of QT (or QTU) interval associated with various types of ventricular tachycardias including BVT. It is inherited in an autosomal dominant manner and is defined as a potassium channelopathy since it is caused by mutations on the *KCNJ2* gene which encodes for the protein Kir2.1. This potassium channel carries a background K-current (called I_{K1}) whose main feature is to maintain a deep resting membrane potential. *KCNJ2* mutations found in ATS usually produce loss-of-function effects and thus induce a subtle depolarization of the resting membrane potential, which in turn increases the resting intracellular Ca level via the Na/Ca exchanger.

In contrast, mutations in genes encoding for either the ryanodine receptor (RyR2) or the Ca-binding protein (CASQ2) have been shown to cause another type of familial arrhythmia, CPVT. CPVT patients have no structural heart defects and show exercise/emotion-triggered syncope and/or sudden cardiac death mainly during childhood. Inheritance also follows an autosomal dominant trait. Proteins encoded by RyR2 or CASQ2 are both important players for Ca handling of the sarcoplasmic reticulum (SR). In fact, several RyR2 mutations have been shown to increase SR Ca-release into the cytoplasm.

Finally, now coming back to digitalis intoxications, the drug is well known to inhibit membrane Na/K-ATPase and eventually increases intracellular Ca concentration via the Na/Ca exchanger. Therefore, increase in intracellular Ca level turns up to be a common feature among these three distinct diseases. Although a precise mechanism underlying this bizarre form of ventricular tachycardia remains unknown, there may be alternative oscillation in cytosolic Ca concentrations in the presence of severe functional failure of Kir2.1, SR Ca-handling, Na/K-ATPase or Na/Ca exchanger, which may in turn affect the

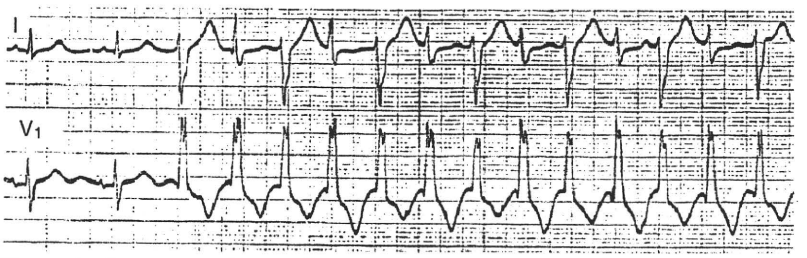

Figure 1 By courtesy of Dr. I Niimura, Yokohama.

morphological ECG features. A computer simulation including intracellular Ca concentrations may offer a clue to answer the mechanistic question in regard to this still-unsolved type of arrhythmia, BVT.

Minoru Horie
Professor,
Department of Cardiovascular Medicine
Shiga University of Medical Science

4

Long QT syndrome with compound mutations is associated with a more severe phenotype: A Japanese multicenter study

Hideki Itoh, MD, PhD,* Wataru Shimizu, MD, PhD,† Kenshi Hayashi, MD, PhD,‡ Kenichiro Yamagata, MD,† Tomoko Sakaguchi, MD, PhD,* Seiko Ohno, MD, PhD,§ Takeru Makiyama, MD, PhD,§ Masaharu Akao, MD, PhD,§ Tomohiko Ai, MD, PhD,¶ Takashi Noda, MD, PhD,† Aya Miyazaki, MD,‖ Yoshihiro Miyamoto, MD, PhD,** Masakazu Yamagishi, MD, PhD,‡ Shiro Kamakura, MD, PhD,† Minoru Horie, MD, PhD*

*From the *Department of Cardiovascular and Respiratory Medicine, Shiga University of Medical Science, Otsu, Japan, †Division of Arrhythmia and Electrophysiology, Department of Cardiovascular Medicine, National Cerebral and Cardiovascular Center, Suita, Japan, ‡Division of Cardiovascular Medicine, Kanazawa University Graduate School of Medical Science, Kanazawa, Japan, §Department of Cardiovascular Medicine, Kyoto University Graduate School of Medicine, Kyoto, Japan, ¶Texas Heart Institute/St. Luke's Episcopal Hospital, Houston, Texas, ‖Department of Pediatric Cardiology, National Cerebral and Cardiovascular Center, Suita, Japan, and **Laboratory of Molecular Genetics, National Cerebral and Cardiovascular Center, Suita, Japan.*

BACKGROUND: Long QT syndrome (LQTS) can be caused by mutations in the cardiac ion channels. Compound mutations occur at a frequency of 4% to 11% among genotyped LQTS cases.

OBJECTIVE: The purpose of this study was to determine the clinical characteristics and manner of onset of cardiac events in Japanese patients with LQTS and compound mutations.

METHODS: Six hundred three genotyped LQTS patients (310 probands and 293 family members) were divided into two groups: those with a single mutation (n = 568) and those with two mutations (n = 35). Clinical phenotypes were compared between the two groups.

RESULTS: Of 310 genotyped probands, 26 (8.4%) had two mutations in the same or different LQTS-related genes (compound mutations). Among the 603 LQTS patients, compound mutation carriers had significantly longer QTc interval (510 ± 56 ms vs 478 ± 53 ms, $P = .001$) and younger age at onset of cardiac events (10 ± 8 years vs 18 ± 16 years, $P = .043$) than did single mutation carriers. The incidence rate of cardiac events before age 40 years and use of beta-blocker therapy among compound mutation carriers also were different than in single mutation carriers. Subgroup analysis showed more cardiac events in LQTS type 1 (LQT1) and type 2 (LQT2) compound mutations compared to single LQT1 and LQT2 mutations.

CONCLUSION: Compound mutation carriers are associated with a more severe phenotype than single mutation carriers.

KEYWORDS Compound; Gene; Long QT syndrome; Mutation

ABBREVIATION QTS = long QT syndrome

(Heart Rhythm 2010;7:1411–1418)

Introduction

Congenital long QT syndrome (LQTS) is a heterogeneous disease characterized by prolonged ventricular repolarization and episodes of syncope and/or life-threatening cardiac arrhythmias, particularly polymorphic ventricular tachycardia.[1] Several disease-causing genes have been identified, including genes encoding cardiac ion channel-composing proteins, namely, *KCNQ1* (LQT1), *KCNH2* (LQT2), *SCN5A* (LQT3), *KCNE1* (LQT5), *KCNE2* (LQT6), *KCNJ2* (LQT7), and *CACNA1C* (LQT8), and genes encoding a family of versatile membrane adapters, namely, *ANK2* (LQT4), *CAV3* (LQT9), *SCN4B* (LQT10), *AKAPs* (LQT11), and *SNTA1* (LQT12).[2–5] Two modes of inheritance are involved in this syndrome, which exhibits both an autosomal dominant and an autosomal recessive pattern. The majority of LQTS cases are inherited in an autosomal dominant fashion. This pattern, which has been named as Romano-Ward syndrome,[6,7] can result from a single mutation in one

Drs. Shimizu, Makiyama, Akao, Miyazaki, Miyamoto, Yamagishi, and Horie were supported in part by a Health Sciences Research Grant (H18-Research on Human Genome-002) and a Research Grant for the Cardiovascular Diseases (21C-8) from the Ministry of Health, Labour and Welfare, Japan. Dr. Itoh was supported in part by a Grant-in-Aid for Young Scientists from the Ministry of Education, Culture and Technology. Dr. Horie was supported by the Uehara Memorial Foundation. Drs. Itoh and Shimizu contributed equally to this study. **Address reprint requests and correspondence:** Dr. Wataru Shimizu, Division of Arrhythmia and Electrophysiology, Department of Cardiovascular Medicine, National Cerebral and Cardiovascular Center, 5-7-1 Fujishiro-dai, Suita, Osaka 565-8565, Japan. E-mail address: wshimizu@hsp.ncvc.go.jp. (Received 7 February 2010; accepted June 3, 2010.)

1547-5271/$ -see front matter doi:10.1016/j.hrthm.2010.06.013